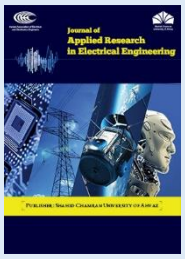
Shahid Chamran University of Ahvaz

Iranian Association of Electrical and Electronics Engineers

Journal of Applied Research in Electrical Engineering

E-ISSN: 2783-2864
P-ISSN: 2717-414X
Homepage: https://jaree.scu.ac.ir/



Research Article

Participation of Virtual Inertia Emulating Constant Power Generating PV Power Plants in Microgrid Frequency Support

Marziye Javadi Sahhaf [1], Arash Khoshooei [2,*]

[1] *Department of Electrical and Computer Engineering, Jundi-Shapur University of Technology, Dezful 61424-18500, Iran*

[2] *Department of Electrical and Computer Engineering, Jundi-Shapur University of Technology, Dezful 61424-18500, Iran*

** Corresponding Author: Khoshooei@jsu.ac.ir*

Abstract: High penetration of Photovoltaic (PV) generation in standalone microgrids challenges frequency stability due to the absence of inherent inertia and limited frequency regulation capability. This paper proposes a coordinated control framework that enables a PV system to provide both inertial response and primary frequency control without using an energy storage system. Inertial response is implemented through a Virtual Synchronous Generator (VSG) control strategy, while primary frequency support is achieved by reserving a portion of the available PV power using Flexible Power Point Tracking (FPPT) in Constant Power Generation (CPG) mode. The main contribution of this work is the integration of VSG-based inertia emulation with FPPT-based power reservation within a unified PV control structure, allowing simultaneous inertial and primary frequency support. Unlike existing approaches, the proposed method preserves the conventional MPPT structure and does not require modification of the DC/DC converter control loop. An adaptive voltage step size is employed to ensure fast convergence to the flexible operating point and robust performance under irradiance variations. Simulation results obtained from a standalone microgrid model in MATLAB/ Simulink® demonstrate fast stabilization of the DC-link voltage, reduced rate of change of frequency, lower frequency deviation, and faster frequency recovery under different scenarios.

Keywords: Constant Power Generation (CPG), Flexible Power Point Tracking (FPPT), Frequency Support, Voltage regulation, Virtual Inertia, Virtual Synchronous Generator (VSG).

Article history
Received 04 August 2025; Revised 28 December 2025; Accepted 10 June 2026; Published online 5 August 2026.
© 2026 Published by Shahid Chamran University of Ahvaz & Iranian Association of Electrical and Electronics Engineers (IAEEE)
How to cite this article
M. Javadi Sahhaf, and A. Khoshooei, " Participation of Virtual Inertia Emulating Constant Power Generating PV Power Plants in Microgrid Frequency Support," *J. Appl. Res. Electr. Eng.*, vol. 4, no. 2, pp. 230-241, 2025. DOI: https://doi.org/10.22055/jaree.2026.50317.1255

Check for updates

1. INTRODUCTION

Today, the utilization of Renewable Energy Sources (RES) like solar energy is increasing rapidly because of economic and environmental opportunities [1]. Due to the DC nature of photovoltaic panels PV systems cannot be connected directly to the power grid. Moreover, dependency of their generation on weather condition leads to variable power generation which creates uncertainty and affects system variables, like bus voltages and grid frequency [2], [3]. Unlike Synchronous Generators (SGs), converter-interfaced DGs (such as photovoltaic and wind units) lack rotating elements or have their mechanical and electrical parts decoupled. As a result, they cannot naturally provide the inertia needed to support or participate in the frequency control of an AC system [4]. Low inertia results in high Rate Of Change Of Frequency (ROCOF) and high frequency deviation. In addition, it may degrade the frequency stability and reliability of the power electronics-based systems [5]. This problem can be solved using the concept of Virtual Synchronous Generator (VSG).

The VSG control algorithm is a control feature that can be added to a power converter controller to behave like an SG [4]. In [4-7] the VSG control structures and various schemes of its implementation are described in detail. In [8-11], there are also control structures that present the concept of VSG as a PV-STATCOM controller.

For the participation of the PV system in frequency support, it is necessary to reserve a part of available power, so that a flexible power can be produced. There are two ways of realization of flexible active power. The first method is to

install an Energy Storage System (ESS) [12]. Reference [13] demonstrates the operation of a PV system that employs VSG technology and an ESS to support the grid via frequency regulation. A control method which improves the stability of the network in the conditions of variable load and radiation is proposed [14]. In [15], a control structure based on VSG is proposed for an islanded microgrid consisting of PV system and ESS aiming to increase the voltage and frequency stability. All the strategies discussed above require an energy storage system, which is generally not economical because of its high upfront cost and limited lifetime caused by intensive charge–discharge operation. The other alternative method to achieve flexible active power, is the Flexible Power Point Tracking (FPPT) algorithm. The FPPT algorithm means moving away the operating point of the PV array from the Maximum Power Point (MPP) based on the required power reserve level [12,16]. This method is economical and does not require any hardware components. FPPT algorithm is implemented in three ways which are known as: i) Power Limiting Control (PLC) or Constant Power Generation (CPG), ii) Power Reserve Control (PRC) and iii) Power Ramp Rate Control (PRRC) [16]. The purpose of the CPG control strategy, is to limit the PV output power to a certain level of power [16,17]. In this way, a percentage of the available power can be reserved. It should be noted that the use of the CPG method is effective when there are many solar power plants so that the amount of power reserve is divided between all power plants. As a result, each small-scale solar power plant reserves a minimum amount of its power capacity. This issue is important from an economic and engineering point of view. There are many studies in the field of constant power generation. In [16,17], control methods of achieving CPG performance are proposed. In [18], a review and comparison of several FPPT algorithms has been introduced. An adjustable constant power generation control scheme for PV clusters connected in a microgrid is proposed in [19]. In [20], a multi-mode FPPT algorithm is proposed with CPG operation. The main advantage of this algorithm compared to the previous works is fast dynamics, low power fluctuations in steady state and less complexity in implementation. This study is focused on presenting an FPPT algorithm and does not discuss about frequency support. An FPPT algorithm (CPG method) with recovery approach in distributed photovoltaic systems is proposed to support the network frequency in [21]. However, complete information (i.e., the degree of algorithm implementation complexity, etc.) of the used FPPT algorithm is not provided. In addition, DC link voltage stabilization and analyzing the Total Harmonic Distortion (THD) of the inverter output current in microgrid which are critical issues, are not discussed in this study. Very few studies have been done to use the CPG algorithm in the PV system for its participation in the frequency support. An inertia-aware adaptive frequency support strategy for distributed photovoltaic systems that jointly adjusts power reserve and dynamic response parameters based on real-time system inertia is presented in [22].

In our study, we aim to propose a structure for the participation of the PV system in standalone microgrid frequency support using VSG technology with conjunction the FPPT algorithm with focus on CPG method. In this work, by modifying the MPPT algorithm, the control scheme tracks the Flexible Power Point (FPP) instead of the MPP in order to achieve limited (constant) power. The objective is that in case of load change or sudden outage of diesel generators, beside the reducing of ROCOF and frequency deviation, rapid restoration of the microgrid frequency is achieved as well. Also, analyzing the effect of FPPT algorithm and VSG technology (each independently) on microgrid frequency support is one of the main objectives of this research. In this structure, no ESS is employed. Furthermore, the use of a VSG control scheme enables microgrid synchronization without relying on a Phase-Locked Loop (PLL). Finally, the effectiveness of the proposed control strategy is validated through MATLAB/Simulink simulations of a standalone microgrid comprising a PV array, diesel generators, and local loads.

The paper is arranged as follows. An overview of the VSG concept is presented in Section 2. The performance of the FPPT algorithm is explained in section 3. In section 4, the analysis of the proposed microgrid configuration is discussed. The simulation of the proposed structure under different scenarios is done in section 5. Finally, the conclusion is presented in section 6.

2. Overview of Virtual Synchronous Generator (VSG)

VSG concept is a combination of control algorithms, renewable energy sources, energy storage systems and power electronics that emulate the inertia of a conventional power system [6].

The Virtual Synchronous Generator (VSG) idea first introduced in 2007 by Beck and Hesse [5]. In general, the VSG technology is derived from the characteristics of the SG (inertia, damping, etc.). From the perspective of power system stability, inertia is the ability to maintain rotor speed and frequency when disturbances occur. When any disturbance causes a power imbalance between generation and the load, the rotor releases or stores kinetic energy corresponding to inertia to resist the frequency deviation. This function is represented by the swing equation of the SG. Another important characteristic of SG is damping. Damping is mainly done by damper bars or armature winding in SG. During small disturbances, the rotor of the generator undergoes speed deviation. In this situation, the damper bars play an important role in rotor synchronization and show damping effect in SG.

2.1. Mathematical model of SG

The mathematical model of SG includes electrical and mechanical parts. The electrical part is the KVL equations related to the armature winding. The mechanical part is responsible for generating angular velocity and θ angle based on the swing equation. The mathematical model of the SG is based on Fig. 1, and is expressed in the form of equations (1)-(5).

$$E_a - v_a = R_{sa} \cdot i_a + L_{sa} \cdot \frac{di_a}{dt} \quad (1)$$

$$E_b - v_b = R_{sb} \cdot i_b + L_{sb} \cdot \frac{di_b}{dt} \quad (2)$$

$$E_c - v_c = R_{sc} \cdot i_c + L_{sc} \cdot \frac{di_c}{dt} \quad (3)$$

$$J\frac{d\omega}{dt} = \frac{P_m - P_e}{\omega} - D(\omega - \omega_0) \quad (4)$$

$$\theta = \int \omega . dt \quad (5)$$

In (1)-(3), E_a, E_b, and E_c are the induced electromotive forces; v_a, v_b, and v_c are the PCC voltages and i_a, i_b, and i_c are also the measured currents at PCC. which are measured values. The symbols R_s and L_s represent the three phase armature resistances and the armature inductances, respectively. In (4) (which is the swing equation), the inertia is denoted by J; the mechanical power is denoted by P_m , and the electrical power is represented by P_e. The damping coefficient is denoted by D. In (5), ω is the angular speed and the phase voltage angle is represented by θ.

2.2. Mathematical model and control loops of VSG algorithm

VSG algorithm consists of two control loops of active power/frequency (P-f) and reactive power/voltage (Q-V). The main part of VSG is the swing equation of the SG. The VSG swing equation [2] is depicted in (6).

$$P_m - P_e = J\omega_{VSG}\frac{d\Delta\omega}{dt} + \omega_{VSG}K_{TD}\Delta\omega \quad (6)$$

Where P_m is the inverter input power (DC side power) in a similar way to mechanical power in SG. P_e is the inverter output power or electrical power (AC side power); J and K_{TD} are virtual moment of inertia and damping torque coefficients, respectively.

$$\Delta\omega = \omega_{VSG} - \omega_0 \quad (7)$$

In (7), ω_{VSG} and ω_0 are the angular speed of the virtual synchronous generator and the reference angular speed, respectively. Equation (7) is a nonlinear model due to $\omega_{VSG}\frac{d\Delta\omega}{dt}$ term. Nevertheless, for small disturbances, the variation of frequency is considered as low enough to assume that $\omega_{VSG} \approx \omega_0$, which leads to [2]:

$$P_m - P_e = J\omega_0\frac{d\Delta\omega}{dt} + \omega_0 K_{TD}\Delta\omega \quad (8)$$

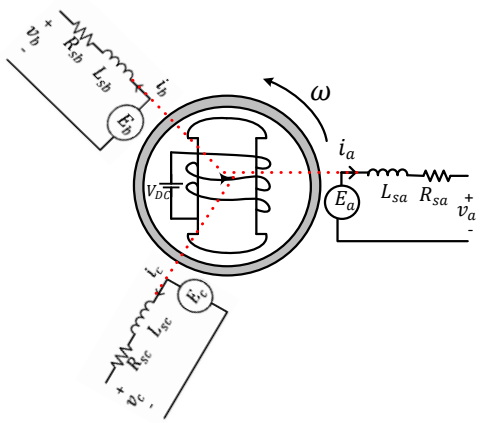


Fig. 1: Simplified SG model.

Finally, by defining M as Virtual Inertia and D as damping coefficient, equation (8) is represented as follows:

$$P_m - P_e = M\frac{d\Delta\omega}{dt} + D\Delta\omega \quad (9)$$

It is clear that the control loop created based on equation (9), plays the role of the rotor and governor of the synchronous generator and is known as active power-frequency (P-f) droop control [23-25]. With equation (9), which emulates the initial frequency regulation as well as damping and inertia of SG, the reference phase angle θ and the frequency of the modulation reference signal could be extracted. The phase angle and angular velocity would be used to transfer the voltages and currents of natural frame to the synchronous reference frame (d-q).

The basic structure of VSG is illustrated in Fig. 2. Primary frequency regulation and virtual inertia fulfillment are among the achievements of the P-f control loop implementation. According to the P-f control loop, when the produced power (P_m) and the demand (P_e) are equal, the frequency of VSG is equal to the nominal frequency of the network. Consequently, the system is stable and synchronous. Existence of a difference between P_m and P_e due to a load increase, makes P_e greater than P_m. Therefore, a frequency droop occurs in the microgrid and the frequency profile fluctuates. At the beginning of frequency deviation, provides inertial support for the system by injection more active power and improves the transient state of the system. Then, recovers the frequency of the microgrid using the initial frequency regulation.

In the load reduction mode, which increases the network frequency, the control system will provide a response in the opposite direction.

Equation (10), is used to calculate the amplitude of the modulation reference signal:

$$k\frac{dE}{dt} = Q_m - Q_e + K_q(V_r - V) \quad (10)$$

In (10), V, V_r , Q_e and Q_m are output voltage, nominal voltage, calculated reactive power and reference reactive power,

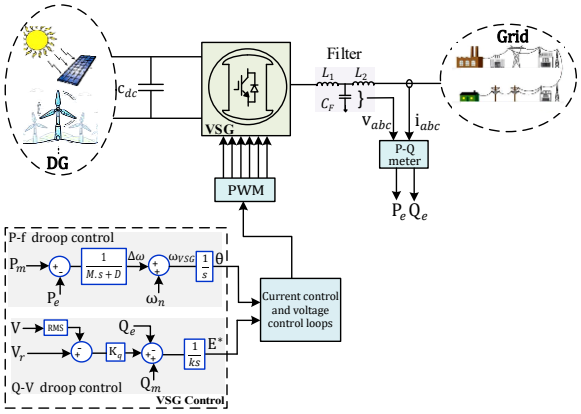


Fig. 2: Basic structure of VSG.

respectively. K_q, k, and E are the droop coefficient, inertia coefficient, and reference output voltage amplitude (virtual Electro Motive Force (EMF)), respectively.

Block diagram representation of equation (10) is shown in Fig. 2, which is called reactive power/voltage (Q-V) droop control. The Q-V droop control loop, plays the role of Automatic Voltage Regulation (AVR) function in SG.

3. CONSTANT POWER GENERATION (CPG) ALGORITHM

The main task of CPG control strategy is to limit the output power of PV array to a certain power level. This control function can be used to avoid overloading the network. This allows more PV systems to be connected to the grid without needing for grid expansion. In addition, by using the CPG strategy, the PV system could participate in frequency support. This strategy is also called absolute power control or Power Limiting Control (PLC) as well [16].

As it is vivid from the PV array P-V characteristic of Fig. 3, there are two operating Constant Power Points (CPP_L, CPP_R) to achieve a limited power level. The operating point of CPP_L is on the left side of MPP (constant current region) and CPP_R is on the right side (constant voltage region). It is clear that, these operating points have different dynamics which, should be considered in the design of CPG control algorithms. In summary, the main task of the CPG strategy is to limit the power at a desired level by setting the operating point at one of the two CPPs. In the following, some of the variations of CPG control strategy is discussed and at the end a proposed strategy is introduced which, has two operating modes of MPPT and CPG. This algorithm has faster dynamics due to the use of the variable voltage step in the CPG mode. Furthermore, in MPPT mode, any normal MPPT algorithm could be used without any restriction.

3.1. Direct power control

One of the common solutions for CPG control is direct regulation of PV output power through closed-loop power control. In this method, the PV power reference (P_{PV}^*) is derived via passing the MPPT mode power (P_{MPP}) through a saturation block which limits the power to a certain level $of\ P_{CPG}$. In this way, when the PV array extracted power exceeds the power limit, the P_{PV}^* is kept at the limited power level and consequently, CPG control can be reached [16, 17]. In Fig. 4, the block diagram of direct power control is shown.

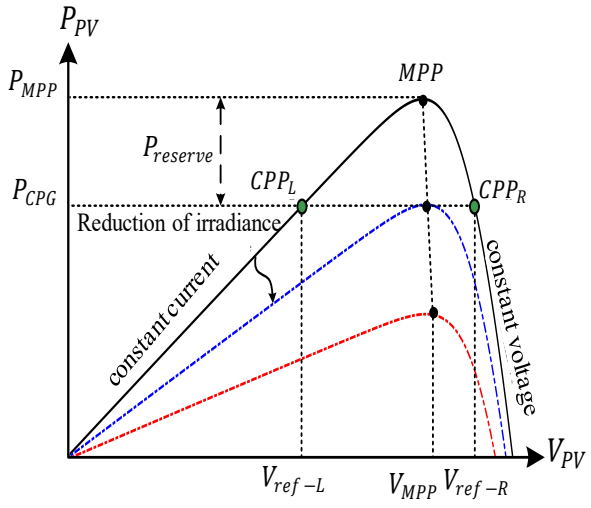


Fig. 3: Possible positions of CPP on the P-V characteristic for CPG control strategy.

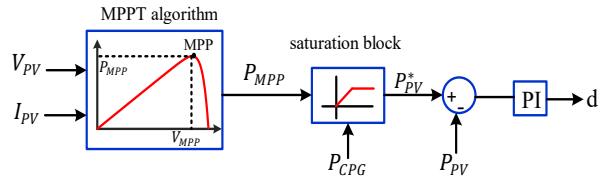


Fig. 4: Block diagram of CPG control with direct power control method.

3.2. Current limiting control

The Power limiting in CPG mode could be achieved by adjusting the output current of the PV. According to the PV array I-V characteristics of Fig. 5, there is an almost constant voltage region on the right side of MPP. Besides, the output current of PV array depends linearly on the solar Irradiance. Therefore, as shown in Fig. 5, limiting the PV output current to a limited current level (I_{CPG}) in the operating area on the right side of the MPP, leads to limiting the PV output power. It should be noted that when the current is used as the control variable, the PV system can only work on the right side of the MPP [16, 17]. The block diagram of CPG control with current limiting method is shown in Fig. 6.

In abovementioned methods, the MPPT algorithm is not altered but the DC-DC converter control loop is modified instead. However, each of the algorithms based on these methods have several defects for the performance of CPG [16,17].

3.3. MPPT algorithm modification method (direct calculation of reference voltage)

Fulfilling the CPG control strategy is also possible by modifying the MPPT algorithms ((P&O) algorithm, etc.). In this method as shown in Fig. 7, to achieve the CPG control

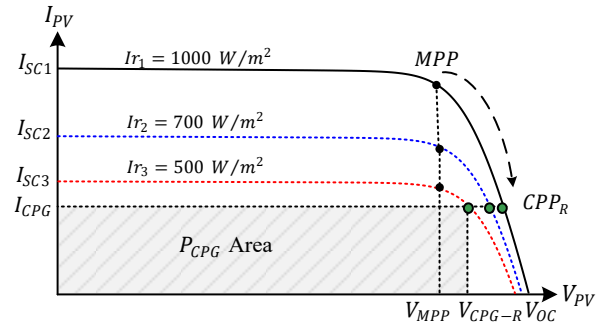


Fig. 5: PV array I-V characteristics.

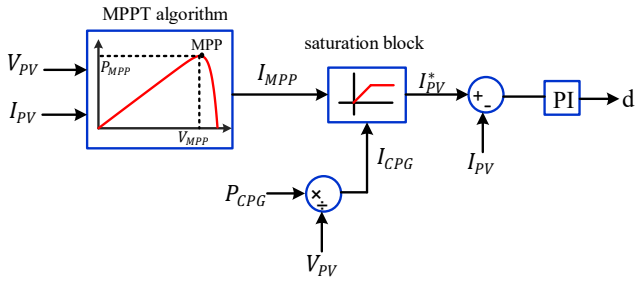


Fig. 6: Block diagram of CPG control with current limiting method.

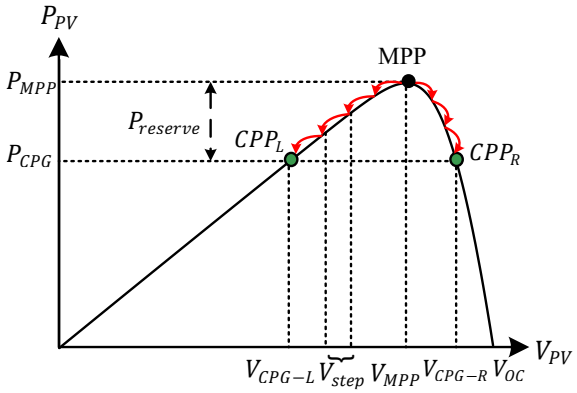


Fig. 7: Behavior of operating points on the P-V characteristic with modified MPPT algorithm.

strategy, the control algorithm should track the CPP instead of the MPP in a similar way as the MPPT algorithm. According to Fig. 7, when the power extracted from the PV array (P_{PV}) is less than the limited power level (P_{CPG}), the PV voltage reference (V_{PV}^*) is determined by the MPPT algorithm. When P_{PV} exceeds P_{CPG}, by disturbing the operating point (i.e., PV voltage (V_{PV})) and moving toward the corresponding CPP (which is P_{CPG}), the PV power would be gradually reduced. Finally, after several time steps, the operating point of the PV array reaches the desired CPP and toggles around it. As the operating point reaches CPP, the PV power reaches P_{CPG} and would be stabilized there.

Fig. 8 shows the block diagram of CPG control with MPPT algorithm modification method. It should be mentioned that with this method in two-stage PV systems, P_{PV} can be adjusted depending on the direction of disturbance in both CPP_R and CPP_L. Each operating point has its own pros and cons, and according to the main objectives of the research, the optimal operating point should be selected. When the PV system is set to operate at the CPP_R point, it provides a faster dynamic performance (compared to the CPP_L operating point); because a small change in voltage results in a large change in power. However, operating on the right side of the MPP (CPP_R) leads to larger power fluctuations compared to the left side of the MPP.

V_{PV}^* is calculated based on (11) and (12), whether the operating point is located on the left side of MPP or on its right side, respectively. V_{step} represents the voltage step in the CPG algorithm.

$$V_{PV}^* = \begin{cases} V_{MPPT} & , \quad when \quad P_{MPPT} \le P_{CPG} \\ V_{PV} - V_{step} & , \quad when \quad P_{MPPT} > P_{CPG} \end{cases} \tag{11}$$

$$V_{PV}^* = \begin{cases} V_{MPPT} & , \quad when \quad P_{MPPT} \le P_{CPG} \\ V_{PV} + V_{step} & , \quad when \quad P_{MPPT} > P_{CPG} \end{cases} \tag{12}$$

All the aforementioned control strategies are able to limit the PV output power according to the set point. However, the MPPT algorithm modification method is a comprehensive and superior scheme.

3.4. Proposed MPPT-CPG algorithm

Compared with the three aforementioned Flexible Power Point Tracking methods, this section introduces an algorithm

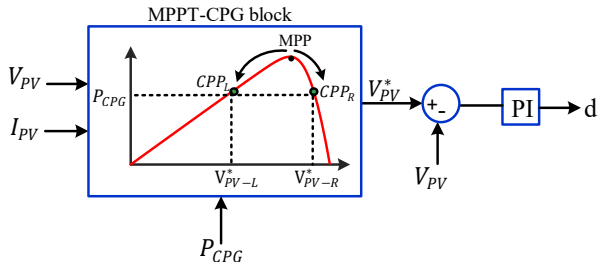


Fig. 8: Block diagram of CPG control with modified MPPT algorithm.

that employs a conventional MPPT scheme and there is no need to modify the control loop of the DC/DC converter. At the same time, employing an adaptive (variable) voltage step size, accelerates convergence to the target operating point, resulting in fast dynamic response in CPG mode and robust performance under irradiance variations.

The flowchart of the proposed MPPT-CPG algorithm is shown in Fig. 9(a). It has two operating modes. First, a conventional MPPT algorithm is implemented to maximize the PV power extraction, while in the second mode, a variable voltage step (ΔV) is used to reduce PV power to the desired limited power value (P_{CPG}). ΔV is calculated by a PI controller. The error signal between P_{PV} and P_{CPG} is fed to the controller. The presence of the PI controller in the proposed algorithm leads to faster dynamics. The larger the error, the larger the ΔV will be. As a result, the operating point moves to the desired point in a shorter time. On the other hand, if the operating point is near the reference point, the error is small and ΔV will be small as well. In this algorithm, the operating point could be chosen to be on the right or left side of MPP. For the sake of faster dynamics, in this research work, the operating point is selected on the right side of the MPP. As it is shown in Fig. 9(a) and the relationship between P_{PV} and P_{CPG}, there are two functional modes:

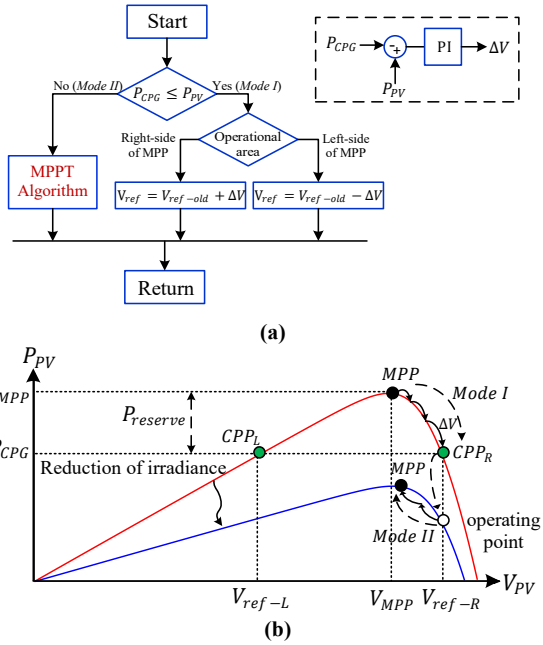


Fig. 9: Proposed MPPT-CPG algorithm: a) flowchart of the proposed algorithm, b) display the operating point trajectory.

- *Mode I* ($P_{CPG} \le P_{PV}$): First, the MPPT algorithm starts to increase the PV power (P_{PV}). When the P_{PV}

is greater than the limited power P_{CPG}, the MPPT algorithm stops and the last stored voltage reference ($V_{ref-old}$) is used. Assuming the selection of the operating region in the right-side of MPP, by adding V_{step} to $V_{ref-old}$ a new voltage (V_{ref}) is obtained; by replacing this voltage, the PV power is reduced.

- *Mode II* ($P_{CPG} > P_{PV}$): If for some reason (e.g., reduction of solar radiation, ect.) the available PV power becomes less than P_{CPG}, in this case, the proposed algorithm increases the PV power towards P_{CPG} by activating the MPPT algorithm.

Fig. 9(b), shows the behavior of the operating point on the right-side of the MPP in both modes. As it illustrated in Fig. 9(b), in Mode I (MPPT algorithm), constant voltage step size and in Mode II (CPG algorithm), variable voltage step has been used.

4. ANALYSIS OF THE PROPOSED MICROGRID CONFIGURATION

In order to evaluate the effectiveness of the proposed MPPT-CPG strategy regarding the participation of the PV system in frequency support with VSG technology, the proposed microgrid configuration is shown in Fig. 10. The microgrid consists of PV power plant, DC/DC boost converter, three-phase inverter (VSG), local loads and a couple of diesel generators. In this research, a double-stage structure is used to connect the PV power plant to PCC. In a double-stage structure, the PV array is connected to the inverter by a DC/DC boost converter. MPPT-CPG algorithm is implemented in the control block of the boost converter.

As it is depicted in Fig.10, the inverter control block is responsible for regulating the DC link voltage (V_{dc}), implementing VSG technology, and controlling the voltage and current of the microgrid. In the following, the description of both the control block of the boost converter and the inverter are presented.

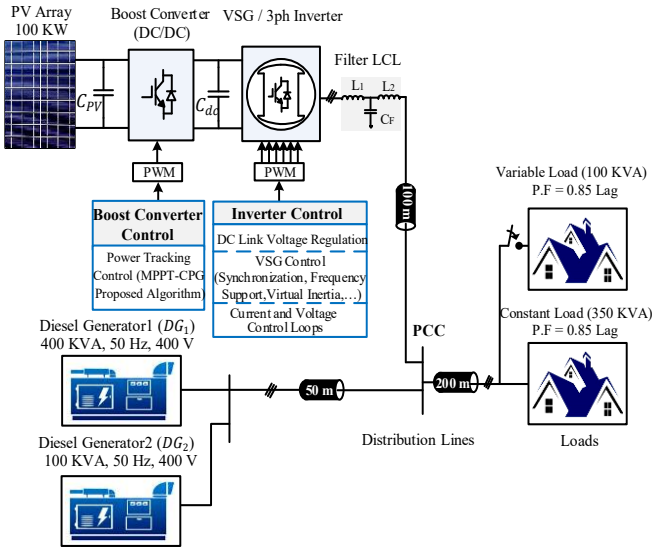


Fig. 10: Proposed microgrid configuration.

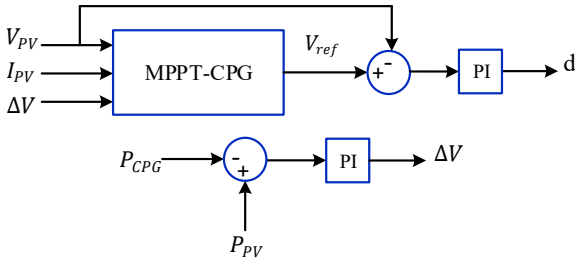


Fig. 11: Boost converter control loop.

4.1. Boost converter control block

The block diagram of the boost converter control is shown in Fig .11. The MPPT-CPG algorithm is implemented in the MPPT-CPG block. The inputs of this block are, the measured PV array terminal voltage (V_{PV}), the measured PV array terminal current (I_{PV}) as well as variable voltage step size (ΔV) (which is used in CPG mode).

ΔV is obtained from the error between P_{PV} and P_{CPG}, which could be positive or negative depending on the value of the powers. The output of the MPPT- CPG block is the reference voltage (V_{ref}), which is an advantage from the point of view of control. Finally, the duty cycle (d) is obtained from the error between V_{ref} and V_{PV}, and fed to the modulator which generates the boost converter gate signal.

4.2. Inverter control block

The inverter (Voltage Source Converter (VSC)) control block consists of three sub-modules. According to the intended control objectives like, VSG algorithm implementation, DC link voltage regulation, and accurate current control for grid support, there are three control loops in the control block. Details of modeling of these control loops will be discussed as follows.

4.2.1. V_{DC} Regulation

It is necessary to set the dc link voltage at a constant value. The control loop of voltage regulation is shown in Fig. 12. The task of this loop is to stabilize V_{dc} at its reference value. Fig. 12 depicts that, a current-type control effort is obtained from the comparison of the measured V_{dc} with its reference value. Due to the presence of the integrator in the PI controller, the obtained value is added to the previous value at each step. Finally, a dc power (P_{dc}) is generated from the product of the control effort and the measured V_{dc}. The operation of the control loop is as follows:

If the measured V_{dc} is greater than the reference voltage, the power is added to the extracted power from the PV array (P_{PV}) and more power is delivered to the grid (the power added to P_{PV} comes from the stored energy in C_{dc}). On the other hand, if the measured V_{dc} is less than the reference value, the error sign is negative and as a result, less power is delivered to the grid.

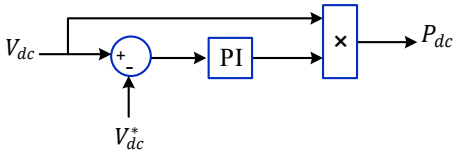


Fig. 12: DC link voltage regulation control loop.

The reduction of V_{dc} means that the energy stored in the capacitor has decreased, which is compensated by the injecting less power to the grid. Finally, if V_{dc} is fixed at the reference value, the PV power will be injected into the inverter with no changes.

4.2.2. VSG Control

In section II, the VSG technology is discussed in detail and here the implementation of VSG control loops is described. As shown in Fig. 2, VSG is composed of the active power/frequency (P-f) droop control loop and the reactive power/voltage (Q-V) droop control loop. The control structure of VSG is shown in Fig. 13. The difference between this structure and the structure of Fig. 2 is in the part of the Q-V droop control loop, which will be discussed in the following.

It is clear from Fig .13(a), that this control loop acts similar to a low-pass filter that does not pass drastic changes and has a smooth movement. From a control point of view, if the system is in a stable state, Δω is zero and ω_{VSG} is equal to ω_n. But if a load increase occurs in the microgrid, Δω becomes negative and as a result, ω_{VSG} would be decreased. In this case, more power (more than P_{CPG}) is delivered from the PV side to the microgrid, as a result, in addition to limiting the frequency excursion, it also restores the frequency. The opposite of this operation occurs in the local load reduction mode.

A control loop is designed to generate the amplitude of the modulated reference signal (Virtual ElectroMotive Force (EMF)) as shown in Fig. 13(b). This structure in another representation of the Q-V droop control loop of Fig. 2.

This structure is simpler than the original structure; it also generates the amplitude of the modulated reference signal (E^*) through the error between the effective value of the PCC voltage (v_{PCC}) and its reference (v^*_{PCC}).

4.2.3. Current and Voltage Control Loops

According to Fig. 14, a three-phase voltage e_{abc} is produced by the oscillator block based on the phase angle θ and amplitude E^* which are created in the VSG control section. By comparing between e_{abc} and v_{PCC} and feeding it to a virtual admittance block, the three-phase reference current (i^*_{abc}) is produced. In order to benefit from simplicity of PI controllers, using a Park's transformation block, the variables are presented in synchronous reference frame. By applying park's transformation showing in equation (13) and (14) on a symmetric three-phase system, the control variables

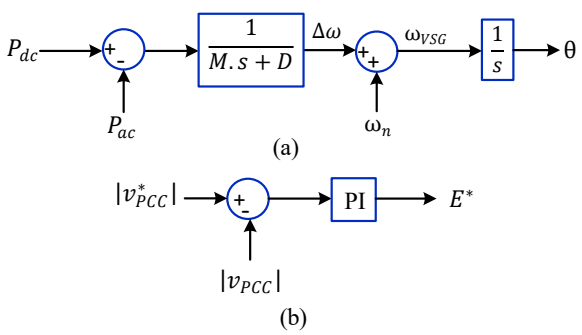


Fig. 13: VSG control loops: a) P-f droop control loop, b) Simplified Q-V droop control loop.

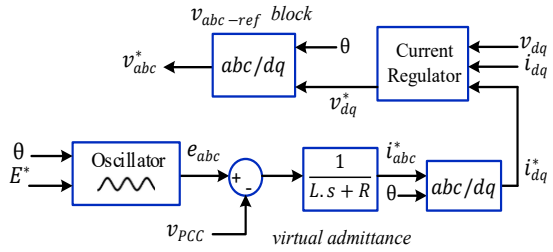


Fig. 14: Current and voltage control loops.

(f_a, f_b, f_c) are converted to a couple of DC components (f_d, f_q) [15].

$$\begin{bmatrix} f_d \\ f_q \\ f_0 \end{bmatrix} = [T_{dq0}(\theta)] \begin{bmatrix} f_a \\ f_b \\ f_c \end{bmatrix} \tag{13}$$

$$[T_{dq0}(\theta)] = \frac{2}{3}\begin{bmatrix} cos(\theta) & cos(\theta - 2\pi/3) & cos(\theta + 2\pi/3) \\ -sin(\theta) & -sin(\theta - 2\pi/3) & -sin(\theta + 2\pi/3) \\ \frac{1}{2} & \frac{1}{2} & \frac{1}{2} \end{bmatrix} \tag{14}$$

The current regulator block shown in Fig. 14. Parameters v_{dq}, i_{dq}, and i^*_{dq} are the PCC voltage, inverter output current, and reference current signals in the synchronous reference frame, respectively. The main purpose of using the current regulator block is to regulate the output current of the inverter by producing a suitable reference voltage.

Finally, v^*_{dq} is converted into a set of three-phase reference voltage (v^*_{abc}) by the $v_{abc-ref}$ block. There is a limiter inside the $v_{abc-ref}$ block, which prevents entering the overmodulation region by limiting the modulation index between zero and one. After producing v^*_{abc} and presenting it to the PWM block, the inverter gate signals are finally produced.

5. Results and Discussion

In this section, to prove the performance of the proposed independent microgrid, simulation of the microgrid under different scenarios has done in MATLAB/Simulink® environment. As it is illustrated in Fig. 10, the PV array, Diesel Generator1 (DG_1) and Diesel Generator2 (DG_2) are sources of energy in this microgrid. A reserved power ($P_{reserve}$) of 0.25 P_{MPP} , for participation of the PV array in supporting the frequency is considered in implementation of the MPPT-CPG algorithm. As a result, in the radiation of $1000\,W/m^2$ and tempretuer of $25℃$, the share of the photovoltaic array in injected power to the microgrid is 75 kW. There are constant and variable local loads as consumers in the microgrid. The important parameters of the simulated microgrid are shown in Table 1.

The first scenario is the solar radiation change scenario with the aim of checking the correct performance of the proposed MPPT-CPG algorithm. The second scenario is the

Table 1: Parameters of the microgrid

Parameters	Values	Parameters	Values
P_{MPP}	100 kW	C_{PV}	1 mF
V_{MPP}	290 V	L	1.5 mH
V_{OC}	363 V	C_{dc}	2 mF
I_{SC}	368.5 A	f_{Sw}	5 kHz
Irr	1000 W/m^2	constant Load	350 kVA
T	25°C	Variable Load	100 kVA
P_{nom}	100 kW	V_{dc}	800 V
V_L	400 V	P_{CPG}	75 kW
i_{Ph}	200 A	L_1	700 µH
f_n	50 Hz	L_2	12 µH
ω_n	$2\pi * f_n$ rad/s	C_F	100 µF
M	$3.14*10^{-3}$	DG_1	400 kVA
D	1.25	DG_2	100 kVA
f_c	10 kHz		

analysis of the effect of VSG and virtual inertia Emulation on frequency support during an increase in the load. After more, scenarios of local load increase and DG_2 outage, (both of which lead to disturbance and frequency droop) are investigated. Finally, the effect of $P_{reserve}$ on the frequency of the microgrid during a load increase scenario is evaluated. It should be mentioned that in this study, the operating point is considered on the right side of the MPP (CPP_R).

5.1. Solar radiation change

In this scenario, the behavior of the MPPT-CPG algorithm and the contribution of the solar power plant and diesel generator in supplying the load when the solar radiation changes are investigated. It should be mentioned that in this scenario, the total installed load in the microgrid is 450 kVA. The curve of solar radiation is shown in Fig. 15(a). According to the Fig. 15(a), at t=7.5s, the radiation has decreased from 1000 W/m^2 to 500 W/m^2 and again increased to 1000 W/m^2 at t=11s. When the radiation decreases to 500 W/m^2, the power extracted from the PV array (P_{PV}) is less than P_{CPG} (75 kW), as a result, based on the algorithm shown in Fig.9, the operating mode is automatically changed to MPPT. In MPPT mode, as shown in Fig. 15(b), the maximum available power in the radiation of 500 W/m^2 is 50 kW. The output active power of DG_1 and DG_2 are shown in Fig. 15(c) and (d), respectively.

When reducing the radiation to 500 W/m^2, DG_1 active power increases from 245 kW to 265 kW and the active power of DG_2 increases from 59 kW to 64 kW for supplying the microgrid load. In short, the participation of the solar power plant in supplying the load is 50 kW, and the rest of the demand is supplied by diesel generators.

At t=11s, the radiation increases again from 500 W/m^2 to 1000 W/m^2. In this case according to Fig. 15(a) and (b), with the increase of radiation, P_{PV} is increased and by the control loop of the boost converter, the operating mode is automatically changed from MPPT to CPG. Finally, the

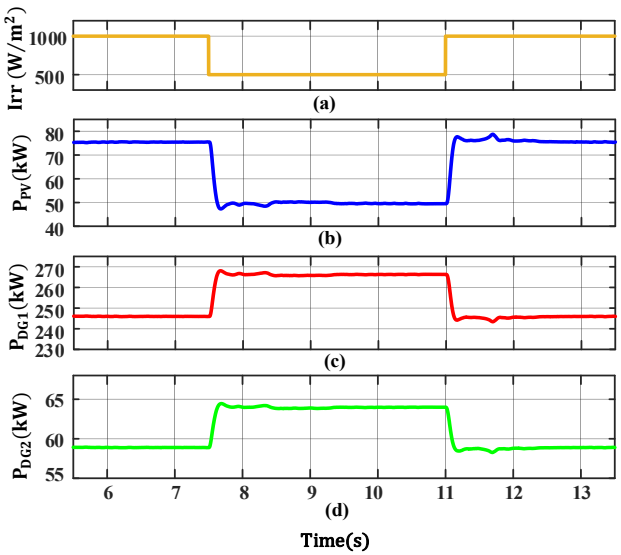


Fig. 15: The contribution of PV power plant and DGs in providing load during solar radiation change: a) Solar radiation, b) Power extracted from the PV array, c) Output active power of DG_1, and d) DG_2 active power.

P_{PV} is limited to the P_{CPG}. In this case, the contribution of PV power plant in load supply is 75 kW and the contribution of DG_1 and DG_2 are 245 kW and 59 kW, respectively, which is shown in Figure 15(c) and (d).

The behavior and trajectory of the operating point during changes in solar radiation are shown in Fig. 16. It is vivid that, in the radiation of 1000 W/m^2, because P_{PV} is more than the constant or limited power (P_{CPG}), the operating point is set at 75 kW (PCC_R). After more, by reducing the radiation to 500 W/m^2, because the P_{PV} is less than the P_{CPG}, based on the proposed algorithm, the operating point moves towards the MPP and upon reaching the MPP point, it settles around it. In the condition of reduced radiation due to the location of the operating point on the right side of the MPP, the PV array voltage must be reduced to move the operating point towards the MPP and increase the power. As the irradiance increases from 500 W/m^2 to 1000W/m^2, the operating mode changes from MPPT to CPG. In this case, the operating point moves towards PCC_R and finally settles around it.

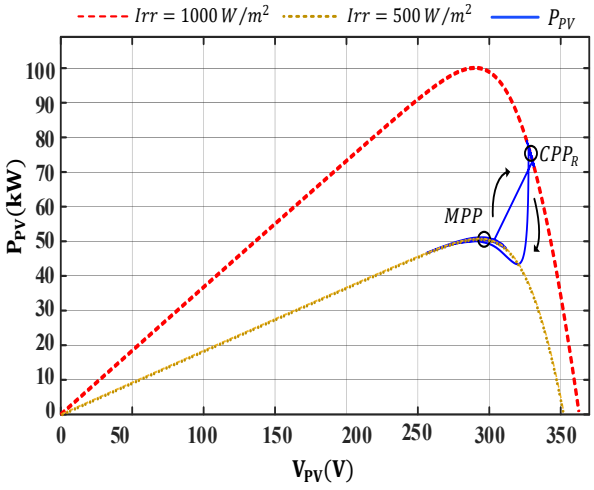


Fig. 16: Operating point trajectory during solar radiation change.

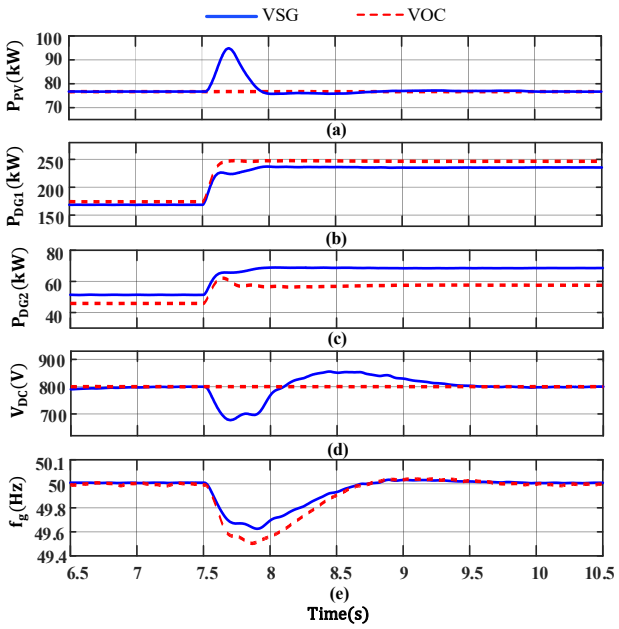


Fig. 17: Simulation results for inverter control in VOC and VSG mode: a) Power extracted from the PV array, b) DG_1 active power, c) DG_2 active power, d) DC link voltage, and e) Microgrid frequency.

5.1. Effect of VSG on frequency support

In this scenario, the effect of virtual inertia emulation on reducing the frequency drop during a load increase scenario is investigated. In this scenario, microgrid simulation is performed for a couple of control modes, first, inverter control based on Voltage Orientation Control (VOC) without inertia emulation or FPPT without VSG and the other, inverter control with inertia mimicry (VSG). Both simulations were conducted under identical conditions. The simulation results are shown in Fig. 17. In t=7.5s, the load increases from 350 kW to 450 Kw. According to Figure 17(a), due to the virtual inertia feature, more energy is injected to the microgrid in VSG mode which prevents a severe frequency deviation. It is vivid from Fig. 17(e), that during the load increase, in VSG mode there is less frequency nadir and RCOF in contrast to VOC mode. To further emphasize the effect of VSG in frequency support, the microgrid frequency curve is shown separately in Fig. 18. It is clear that VSG technology outperforms VOC in frequency support and frequency nadir reduction. Furthermore, ROCOF index is significantly lower in VSG mode with respect to the VOC mode.

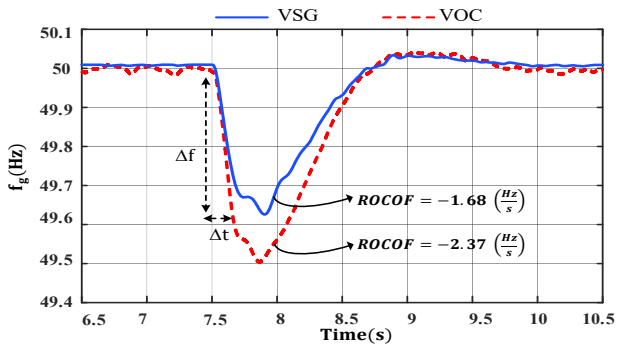


Fig. 18: Microgrid frequency deviation in VOC and VSG mode.

5.2. Load change

In this scenario, the behavior of the microgrid when the load increases from 350 kW to 450 kW is analyzed. Simulations for a comparative examination of the MPPT algorithm and the proposed MPPT-CPG algorithm are conducted. A constant load of 350 kVA is present in the microgrid throughout the simulation process. According to Fig. 19(a), before $t = 7.5\ s$, the system is in steady state and the injected power from the PV array to the microgrid in MPPT-CPG mode is 75 kW (25% of available power is reserved). Also, V_{DC} is stabilized at 800V and the frequency of the microgrid is set at the nominal value of 50 Hz. At $t = 7.5\ s$, a load of 100 kVA is connected to the microgrid and the total load is increased to 450kVA. It is vivid from Fig. 19(d) and (e) that, an imbalance between demand and the produced power happens and consequently, DC voltage drop as well as frequency drop occur in the microgrid. In this situation, VSG algorithm relying on the virtual inertia feature, injects more PV power (Fig. 19(a) MPPT-CPG mode), and hereby, prevents high frequency deviation. Then, frequency restores after a while. According to Fig. 19(e), by using the MPPT-CPG algorithm, the frequency drop as well as the ROCOF experience less values, which is due to the participation of the PV system in the frequency support. Moreover, it is evident from Fig. 19(d) that, thanks to using the proposed algorithm, less DC voltage drop occurs and the voltage settles again at the nominal value (800 V). In a cooperation with PV power plant, part of the load is supplied by DG_1 and DG_2, which is shown in Fig. 19(b) and (c). Fig. 20 shows the trajectory of the operating point when the load increases. As the load increases, the operating point has moved towards MPP to increase the PV power. Because the operating point is selected on the right side of MPP, then decreasing the terminal voltage of the PV array (V_{PV}) will increase the P_{PV}. Subsequently, after a period of time, the operating point returns to CPP_R (75 kW) and the system reaches stability.

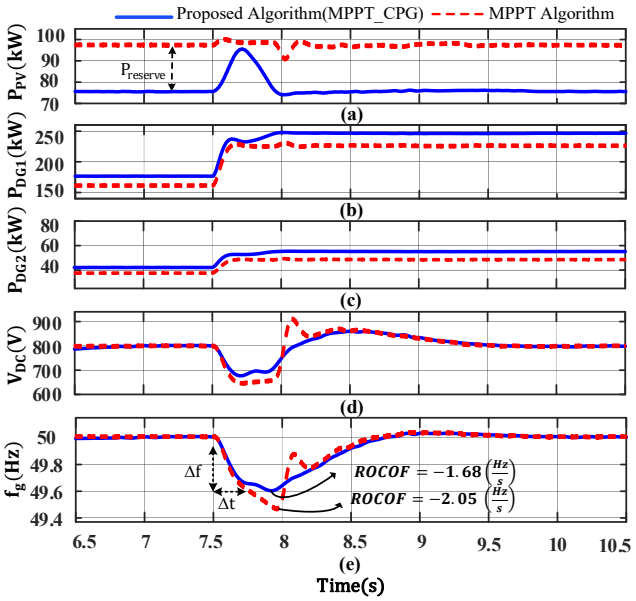


Fig. 19: Simulation results during microgrid local load increase: a) Power extracted from the PV array, b) DG_1 active power, c) DG_2 active power, d) DC link voltage, and e) Microgrid frequency.

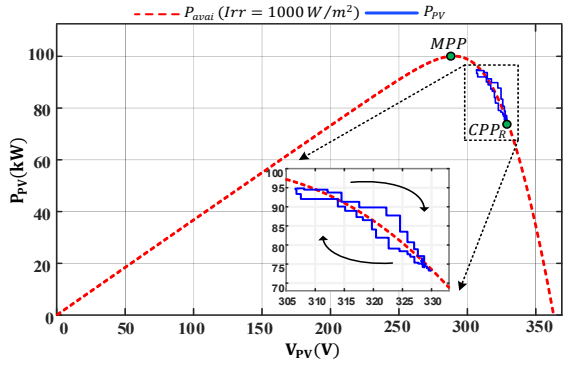


Fig. 20: Operating point trajectory during local load increase.

Fig. 21 shows Q_{VSG}, Q_{DG1} and Q_{DG2} respectively. According to the figure, reactive power of the loads is produced by DGs. To fulfill the PCC voltage regulation, VSG absorbs a small amount of reactive power.

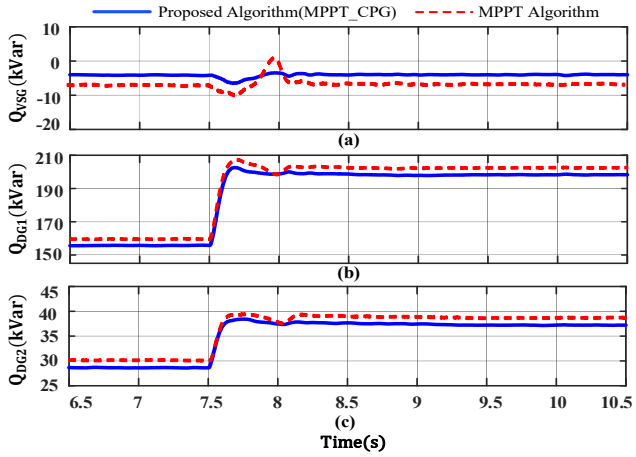


Fig. 21: Reactive power profile during microgrid local load increase: a) VSG output reactive power, b) DG_1 output reactive power and c) DG_2 output reactive power.

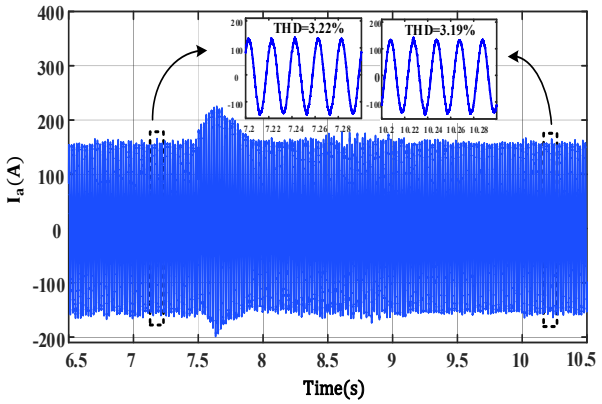


Fig. 22: THD analysis of inverter output current in load change scenario.

Finally, the harmonic content of the current has been analyzed. As stated in Section 1, for a grid connected PV power plant, current Total Harmonic Distortion (THD_i) should be less than 5%. The phase current THD of VSG based PV power plant is shown in Fig. 22. The value of THD before and after increasing the load is less than 5%, and the current waveform has a favorable sinusoidal state.

In Table 2, the Δf, ROCOF, and DC voltage excursion indices for three modes (the proposed algorithm MPPT-CPG with VSG, MPPT-CPG algorithm with VOC (No VSG), and conventional MPPT algorithm) are numerically compared under load increase scenario. It can be clearly proven that the proposed method has lower frequency excursion and ROCOF with respect to the other counterparts. Moreover, MPPT-CPG algorithm with VSG, has lower voltage excursion (with respect to the rated 800 V Voltage) in contrast to the MPPT algorithm. In MPPT-CPG algorithm with VOC, which does not provide virtual inertia support, no energy exchange occurs with the DC link during frequency variations; consequently, the DC-link voltage remains nearly unchanged.

5.3. Diesel generator outage

To investigate the effectiveness of the participation of the PV power plant in frequency support during a possible fault in the microgrid, simulation of sudden outage of DG_2 has conducted. According to Fig. 23(c), the outage occurred in $t = 8\,s$ and the DG_2 output power dropped to zero. In this situation, the P_{PV} in the proposed MPPT- CPG algorithm is increased to participate in frequency support, as shown in Fig. 23(a). It is clear from Fig. 23 (c) and (d) that by the proposed algorithm and VSG technology, not only the voltage drop of the DC link is decreased, but also, less ROCOF and frequency deviation occurs in the microgrid. With the outage of DG_2, DG_1 must generate more power to supply the load demand as shown in Fig. 23(b).

5.4. Effect of photovoltaic power reserve level on microgrid frequency control

One of the advantages of reserving a part of PV power plant available power is to help the stability of the microgrid during peak energy consumption. In this scenario, the effect of the power reservation ($P_{reserve}$) in a photovoltaic power plant on the ROCOF and frequency deviation (Δf) when the load is increased has been discussed. Fig. 24 shows the microgrid frequency for different amount of $P_{reserve}$. According to Fig. 24, the higher $P_{reserve}$ is, the less frequency deviation and ROCOF occurs during the load change. Indeed, by reserving more PV power, more energy can be delivered into the microgrid during frequency deviation Furthermore, to elaborate the correlation of power reservation and frequency deviation, the ROCOF curve as well as Δf curve versus $P_{reserve}$ are shown in Fig. 25. In Fig. 25(b), Δf is obtained from the difference between the nominal frequency and the frequency nadir ($\Delta f = f_n - f_{nadir}$).

In this way, the PV power plant can play an effective role in frequency support.

Table 2: Numerical comparison of Δf, ROCOF, and DC voltage excursion indices

Modes	Δf (Hz)	ROCOF (Hz/s)	ΔV_{DC} (%)
MPPT-CPG algorithm (with VSG)	0.40	-1.67	15.50
MPPT-CPG algorithm (without VSG)	0.50	-2.37	≈0
MPPT algorithm (with VSG)	0.54	-2.05	19.30

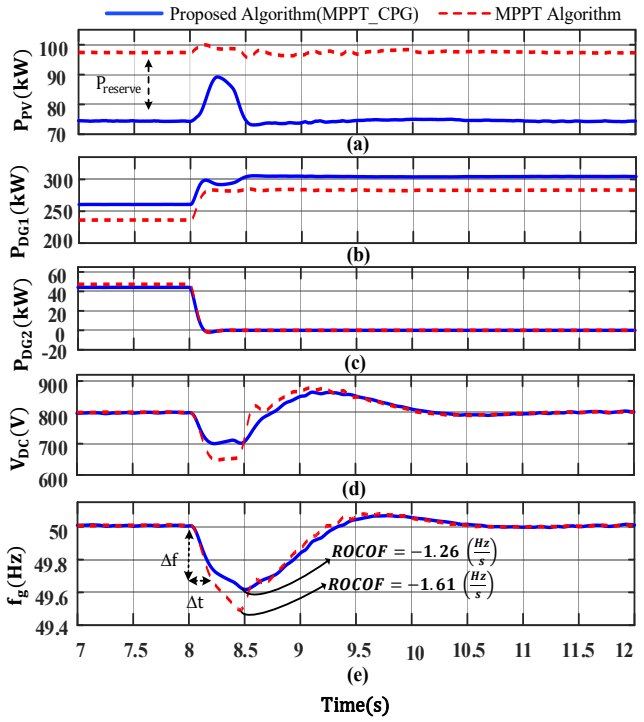


Fig. 23: Simulation results during the diesel generator outage: a) Power extracted from the PV array, b) DG_1 active power, c) DG_2 active power, d) DC link voltage, and e) Microgrid frequency.

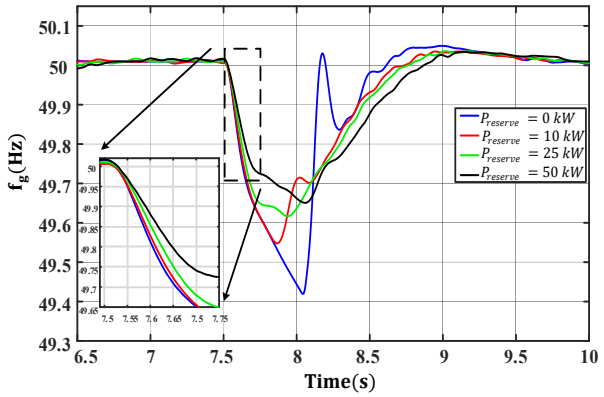


Fig. 24: Effect of $P_{reserve}$ level on the frequency support of microgrid during load increase.

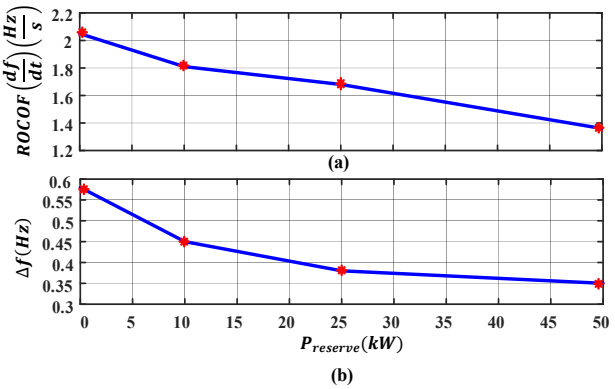


Fig. 25: ROCOF curve and Δf curve in terms of $P_{reserve}$: a) ROCOF curve in terms of $P_{reserve}$, b) Frequency deviation (Δf) curve in terms of $P_{reserve}$.

6. CONCLUSION

This paper demonstrated that a photovoltaic (PV) power plant can actively contribute to both inertial response and primary frequency control in a standalone microgrid through the coordinated application of Virtual Synchronous Generator (VSG) control and an MPPT–CPG based Flexible Power Point Tracking strategy, without relying on an energy storage system. The results confirm that reserving active power within the PV system enables effective frequency support that is traditionally provided by synchronous generators or storage-equipped converters. Beyond validating frequency support capability, the study reveals that the reserved power level plays a decisive role in shaping the microgrid's dynamic frequency response. Increasing the reserve margin consistently improves frequency nadir, reduces the rate of change of frequency (ROCOF), and mitigates DC-link voltage excursions during load disturbances and generator outages. This highlights an inherent trade-off between energy harvesting and frequency stability that can be explicitly managed through the proposed control framework. Overall, the proposed approach provides a practical and storage-free solution for enhancing frequency stability in standalone microgrids with high PV penetration. The findings offer valuable design insights for selecting appropriate power reserve levels and demonstrate the feasibility of integrating inertia emulation and primary frequency control within conventional PV converter structures.

REFERENCES

[1] H.Karimi, M. M. Bidgoli, S. Jadid, "Optimal electrical, heating, cooling, and water management of integrated multi-energy systems considering demand-side management," *Electric Power Systems Research*, vol. 220, article 109353, 2023.

[2] W. Gao, "Control Strategy for a Small-Scale Microgrid Based on Battery Energy Storage System-Virtual Synchronous Generator (bess-Vsg)," Ph.D. Thesis, University of Denver, 2019.

[3] A. Morsagh Dezfuli , M. Abasi , M. E. Hasanzadeh and M. Joorabian, "Voltage and Frequency Control Considering Disturbance in Input Power of DG," *Journal of Applied Research in Electrical Engineering*, vol. 3, no. 1, pp. 9-18, 2024.

[4] C. Liyanage, I. Nutkani and L. Meegahapola, "A Comparative Analysis of Prominent Virtual Synchronous Generator Strategies Under Different Network Conditions," in *IEEE Open Access Journal of Power and Energy*, vol. 11, pp. 178-195, 2024.

[5] M. Chen, D. Zhou, F. Blaabjerg, "Modelling, implementation, and assessment of virtual synchronous generator in power systems," *Journal of Modern Power System*, Clean Energy, vol. 8, pp. 399-411, 2020.

[6] M. Chethan and K. Ravi, "Virtual Inertia Support for Renewable Energy Integration: A Review," in *IEEE Access*, vol. 13, pp. 11517-11531, 2025.

[7] R. Arjmandzadeh, M. Banejad and A. Akbarzadeh Kalat, "Improving the Performance of a VSG in the Distorted Grid Using Third-Order Generalized Integrator," *Journal of Applied Research in Electrical Engineering*, vol. 3, no. 1, pp. 1-8, 2024.

[8] C. Li, R. Burgos, I. Cvetkovic, D. Boroyevich, L. Mili, P. Rodriguez, "Analysis and design of virtual synchronous machine based STATCOM controller," *IEEE 15th Workshop Control and Model Power Electronics (COMPEL)*, Santander, Spain, pp. 1-6, 2014.
[9] N. Kumar, O. N. Buwa, M. P. Thakre, "Virtual synchronous machine based PV-STATCOM controller," in 2020 *IEEE First International Conference on Smart Technologies for Power, Energy and Control (STPEC)*, Nagpur, India, 2020 ,pp. 1-6.
[10] M. P. Thakre, N. Kumar, "Evaluation and control perceptive of VSM-based multilevel PV-STATCOM for distributed energy system," *MAPAN Jornal of Metrology Society of India,* vol. 36, pp. 561-578, 2021.
[11] S. Yazdani, M. Ferdowsi, P. Shamsi, "Virtual inertia based control of PV-STATCOM: operation under unbalanced frequency and grid conditions," in 2020 *IEEE Kansas Power and Energy Conference (KPEC)*, Manhattan, KS, USA, 2020, pp. 1-4.
[12] C. Zhong, Y. Zhou, X. P. Zhang, G. Yan, "Flexible power-point-tracking-based frequency regulation strategy for PV system," *IET Renewable Power Generetion*, vol. 14, pp. 1797-1807, 2020.
[13] H. Xu, J. Su, N. Liu, Y. Shi, "A grid-supporting photovoltaic system implemented by a VSG with energy storage," *Energies*, vol. 11, pp. 1-19, 2018.
[14] X. Yan, C. Wang, Z. Wang, H. Ma, B. Liang, X. Wei, "A united control strategy of photovoltaic-battery energy storage system based on voltage-frequency controlled VSG," *Electronics*, vol. 10, pp. 1-17, 2021.
[15] M. Mao, C. Qian, Y. Ding, "Decentralized coordination power control for islanding microgrid based on PV/BES-VSG," *CPSS Transactions on Power Electronics and Applications*, vol. 3, pp. 14-24, 2018.
[16] Y. Yang, K. A. Kim, F. Blaabjerg, A. Sangwongwanich, "Advances in grid-connected photovoltaic power conversion systems," *Woodhead Publishing an Imprint of Elsevier*, pp. 153-183, 2019.
[17] A. Sangwongwanich, J. He, Y. Pan, "Chapter 15 - Advanced power control of photovoltaic systems, *Control of Power Electronic Converters and Systems*, Academic Press , 2021,pp. 447-469.
[18] H. D. Tafti, G. Konstantinou, C. D. Townsend, G. G. Farivar, A. Sangwongwanich, Y. Yang, J. Pou, F. Blaabjerg, "Extended functionalities of photovoltaic systems with flexible power point tracking: recent advances," *IEEE Transactions on Power Electronics*, vol. 35, pp. 9342-9356, 2020.
[19] H. D. Tafti, A. Sangwongwanich, Y. Yang, G. Konstantinou, J. Pou, F. Blaabjerg, "A general algorithm for flexible active power control of photovoltaic systems," *in 2018 IEEE Applied Power Electronics Conference and Exposition (APEC)*, 2018, pp. 1115-1121.
[20] H. D. Tafti, C. D. Townsend, G. Konstantinou , J. Pou, "A multi-mode flexible power point tracking algorithm for photovoltaic power plants," *IEEE Transactions on Power Electronics*. vol. 34, pp. 5038-5042, 2019.
[21] H. D. Tafti, G. Konstantinou, J. E. Fletcher, L. Callegaro, G. G. Farivar, J. Pou, "Control of distributed photovoltaic inverters for frequency support and system recovery," *IEEE Transactions on Power Electronics*, vol. 37, pp. 4742-4750, 2022.
[22] H. D. Tafti, G. Konstantinou, Q. Lei, J. E. Fletcher, G. G. Farivar, S. Ceballos, Josep Pou, "Adaptive power system frequency support from distributed photovoltaic systems," *Solar Energy*, vol. 257, pp. 231-239, 2023.
[23] Z. Lan, J. Wang, J. Zeng, D. He, F. Xiao, F. Jiang, "Constant frequency control strategy of microgrids by coordinating energy router and energy storage system," *Mathmatical Problems in Engineering*, pp. 1-8, 2020.
[24] X. Ding, T. Lan, H. Dong, "Control strategy and stability analysis of virtual synchronous generators combined with photovoltaic dynamic characteristics," *Journal of Power Electronics*, vol. 19, no. 5, pp. 1270-1277, 2019.
[25] L. Yang, J. Gan, C. Xia, Z. Hu, B. Gao, L. Qu, "Research on the frequency regulation strategy of virtual synchronous generator based photovoltaic power plant," *in 2018 IEEE 8th Annual International Conference on CYBER Technology in Automation, Control, and Intelligent Systems (CYBER)*, (2018), pp. 1305-1310.

BIOGRAPHY



Marziye Javadi Sahhaf received her B.Sc. degree in Electronic Engineering in 2020 and her M.Sc. degree in Power Electronics Engineering in 2023, both from Jundi-shapur University of Technology, Dezful, Iran. Her research interests include the modeling and control of microgrids and power electronics.



Arash Khoshooei received his B.Sc. in Power Engineering from Shahid Chamran University, Ahvaz, Iran in 2001 and M.Sc. (2004) and Ph.D. (2018) degrees in Power Electronics from the Amirkabir University of Technology (AUT), Tehran, Iran. From 2015 to 2016, he was a visiting researcher at the Technical University of Catalonia (UPC), Barcelona, Spain. He is currently a faculty member with the Department of Electrical Engineering at Jundi-Shapur University of Technology. His research interests include modeling and control of power electronics converters and integration of distributed generation systems.

Copyrights
© 2026 by the author(s). Licensee Shahid Chamran University of Ahvaz, Ahvaz, Iran. This article is an open-access article distributed under the terms and conditions of the Creative Commons Attribution –NonCommercial 4.0 International (CC BY-NC 4.0) License (http://creativecommons.org/licenses/by-nc/4.0/).